Proceedings World Geothermal Congress 2010
Bali, Indonesia, 25-29 April 2010

Modeling the Thermal Field and the Impact of Salt Structures in the North East German Basin

Mauro Cacace[1,2] & Magdalena Scheck-Wenderoth[2]

[1]University of Potsdam, Department of Geosciences, Karl-Liebknecht Strasse 24, 14476 Potsdam, Germany

[2] Helmholtz Centre Potsdam GFZ German Research Centre for Geosciences, Telegrafenberg 14473 Potsdam, Germany

cacace@gfz-potsdam.de

Keywords: Numerical simulation, heat and fluid transport, salt structures, geothermal field and surface heat flow

ABSTRACT

Geothermal energy represents by far one of the most extensively used renewable energy worldwide. The long term availability and the large extent of geothermal heat make it an effective source for a sustainable supply of energy. Exploitation of geothermal energy requires a quantitative resource assessment that must provide a correct identification of the main physical transport mechanisms involved. To understand the thermal regime and its interaction with the basin-scale fluid system, as well as its potential for geothermal energy production, three dimensional, basin-scale, numerical simulations of coupled heat, and fluid transport and transfer processes are carried out for the area of the North East German Basin (NEGB) in northern Germany. The main effort of the present study is to build a physically consistent model for the entire basin which integrates the relative impacts of thermal gradients on the regional fluid regime and their coupling with the observed structural and mechanical heterogeneities affecting the basin.

1. INTRODUCTION

Sedimentary basins host a significant portion of the world's economic mineral and energy resources. Formation of these resources involves the interaction of ground-water flow, mechanical deformation, mass transport and transfer as well as heat transport processes. Among the different mechanisms affecting large-scale fluid flow in sedimentary basins, the most influential include: (1) topography/gravity driven flow, (2) tectonically driven flow, (3) compaction driven flow during basin subsidence, and (4) buoyancy driven convective fluid flow. In the last situation the driving forces for the fluid are provided by density gradients as induced by combined effects of temperature and species concentration non uniformities within the fluid saturated medium. All these mechanisms are not exclusive but are strongly coupled. One of the most interesting and most complex examples of these interactions is provided by a mixed convective regime, where the effects of hydraulic gradients and those provided by fluid density gradients are superposed. Understanding the basic physical processes affecting the thermal and fluid regime in porous media when both thermal expansion effects and variations in solute concentration determine variations in fluid density is of particularly economic and societal concern in geothermal basinal systems where groundwater is usually charged by salt in solution. Other applications include ore formations in hydrothermal systems, fluid evolution beneath active volcanic zones as well as brines flows in sedimentary basins. In order to draw general conclusions with regard to the specific problematic related to mixed convection exact analytical solutions when available should be preferred to approximate numerical solutions (e.g. Zhao et al., 2004). The main disadvantage of analytical methods is their limited applicability to real case aquifer settings due to their stringent assumptions. Moreover, the stability criteria relevant to describe these processes are not well understood. As a matter of fact, the classical Rayleigh theory can be successfully used to describe onset and stability conditions for convective flows in homogeneous systems, while it usually fails to predict the occurrence of instabilities under heterogeneous flow conditions (Simmons et al., 2001). This is particularly the situation in simulations of the large-scale (i.e. regional) density-dependent flow where the geometrical and stratigraphic complexities of real case aquifer settings prevent to derive exact analytical solutions. In this regard, numerical solutions represent a useful alternative. Once validated and verified, numerical models provide an important and very often unique tool to elucidate the interrelations between fluid flow mechanisms and complex geometrical and geological settings including heterogeneous material properties. To get a deeper understanding of the different coupled processes affecting if not controlling the thermal regime and the basin-wide fluid system the present study deals with numerical modelling of coupled fluid and heat transport. The 'natural laboratory' is the North East German Basin (NEGB) in northern Germany (see Figure 1).

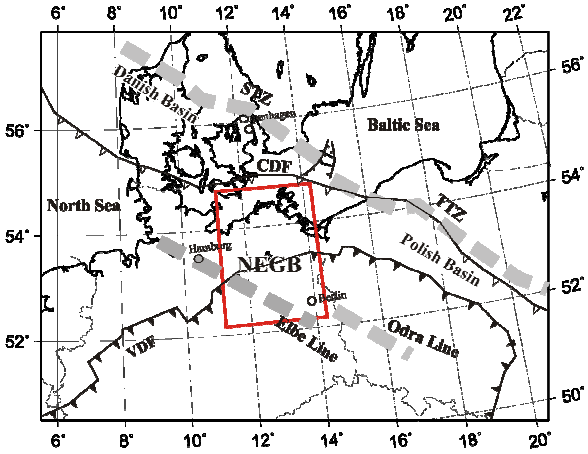

Figure 1: Location of the study area (red frame) in its regional tectonic framework, modified after Bayer et al. (1999). Abbreviations: STZ=Sorgenfrei Tornquist Zone; TTZ= Teisseyre Tornquist Zone; VDF= Variscan Deformation Front; CDF= Caledonian Deformation Front

The NEGB as a part of the North German Depression is located north of the Elbe Fault System (EFS) and south to the Tornquist-Teisseyre Zone (TTZ) and the Caledonian

deformation Front (CDF). The basin succession ranges in age from Permian (about 300 Ma) to Quaternary with a thickness of deposits reaching up to 8 km (Bayer et al., 1999). The NEGB provides an interesting example for a natural geothermal system where to investigate all the aforementioned processes. It is interesting since its recent structural setting is mainly controlled by the presence of a thick sequence of Zechstein salt highly structured by many salt diapirs and pillows, see Figure 2.

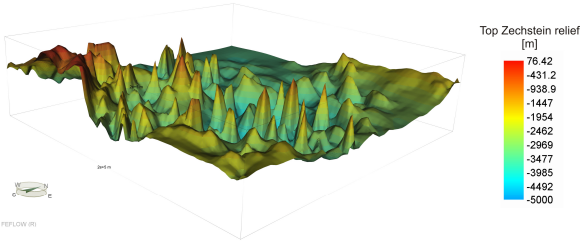

Figure 2: Relief of the top Zechstein salt, after Scheck (1997)

Apart from acting as a mechanical decoupling horizon between the supra salt (Mesozoic and Cenozoic sedimentary successions) and the sub salt (Upper Permian pre Zechstein sedimentary deposits), these salt structures strongly modify the regional thermal field within the basin. Due to the strong contrast in thermal conductivity between salt rocks relative to the surrounding clastics and carbonates, salt modifies the long-term (i.e. conductive) spatial temperature distribution. Additionally these salt structures may be considered responsible for the presence of an active convective system as also constrained by hydro-geochemical studies, Magri et al. (2005) and references therein. This basin-wide convective system may explain the 'anomalous' temperature and heat flow distribution within the basin, where regions of higher than expected heat flow values observed at the near surface (up to 90 mWm^{-2}, e.g. Hurtig et al., 1992; Norden et al., 2008) does not seem to spatially correlate with the geometry and thickness of the sedimentary infill. Most likely these local and small-scale deviations in the surface heat flow distribution may result from the effects of deep rooted groundwater flow. Despite of this, previous thermal studies in the NEGB either were restricted to account for basin-scale conductive energy processes (e.g. Bayer et al., 1997) or considered both flow transport mechanisms for specific two dimensional profiles (e.g. Magri et al., 2005). New in this study is to carry out three dimensional, basin-wide numerical investigations of the fully coupled fluid flow and heat transport mechanisms. The aim of the study is twofold. Based on a detailed structural model of the basin, in the first part of the study the recent regional geothermal field is modeled. This analysis enables to quantify the interaction of the different physical thermal rock properties and the thickness of the main structural layers with regard to the resulting steady-state conductive thermal field and background surface heat flow distribution. New available data on both the thermal and heat flow structure as obtained during the last tow decades are used to better constrain modeling results. This first study provides proper and essential boundary conditions as well as reliable physical constraints to be used in more refined and more complex models. Numerical solutions of the coupled equation of fluid flow and heat transport are then used to quantify the effects of groundwater flow on the subsurface thermal regime and to get deeper insights in the structure and details of the convective flow system affecting the basin.

2. RECENT STEADY-STATE GEOTHERMAL FIELD

In the first part of the study the recent thermal regime in the subsurface of the NEGB is modeled. The aim of the study is (a) to develop a numerical model for the recent thermal structure of the NEGB on a lithospheric scale, and (b) to investigate the feed back of parameters changes (thermal rock properties and thickness of the lithospheric layers) on the temperature and heat flow distribution. At the same time, estimating the undisturbed conductive heat flow at the base of the NEGB provides important boundary conditions as well as physical constraints for numerical studies on the coupled fluid and heat flow, a subject that will be tackled in the next section. The basis of the study is provided by a detailed three dimensional structural model of the basin used to describe the geometry as well as to constrain the lithologically dependent thermal properties of rocks. The geological structure and nature of the sedimentary section has been integrated in the current study following the work by Scheck (1997). It consists of 13 different sedimentary layers from Lower Permian to Cenozoic strata (see Figure 3).

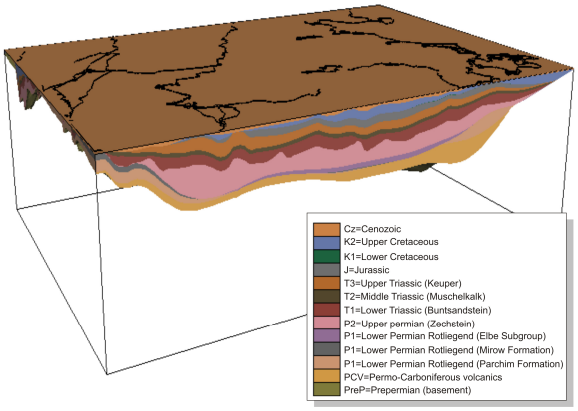

Figure 3: Geometries of the Lower Permian to Cenozoic sedimentary sequence considered in the study, modeled after Scheck (1997)

The area covered by the model is 230 × 330 km in the horizontal extensions. The resolution of the model is approximately 4 km horizontally, while it varies vertically according to the variable thickness of the sedimentary units. The relative high resolution of the model enables to represent details of the different salt structures affecting the study area. The deeper structures comprise a two layered crust underlying the basement of the sediment infill. The respective thickness of the crustal layers are derived by newly available Moho depth maps as published by Tesauro et al., 2008 (see Figure 4) and constraints provided by other geophysical data derived from gravity and seimics. The lowermost layer of the model is represented by a thermal mantle lithosphere of variable thickness, see the discussion below. Assuming a stable steady-state thermal regime and heat conduction as the main energy transfer mechanism, the relevant energy equation

$$\nabla \cdot (\boldsymbol{\lambda} \nabla T) = -H \,, \qquad (1)$$

(with $\boldsymbol{\lambda}$ [$W(mK)^{-1}$] rock thermal conductivity tensor and H [Wm^{-3}] radiogenic heat production) is numerically solved by means of a 3-D FEM procedure as described in detailed by Bayer et al. (1997). In this first study, no additional transient component as related to heat convection, mass transport and/or active mantle thermal activities are considered. The boundary conditions adopted are a constant temperature of 8 °C at the top surface of the model which

corresponds to the average temperature as observed at the surface for the area under consideration.

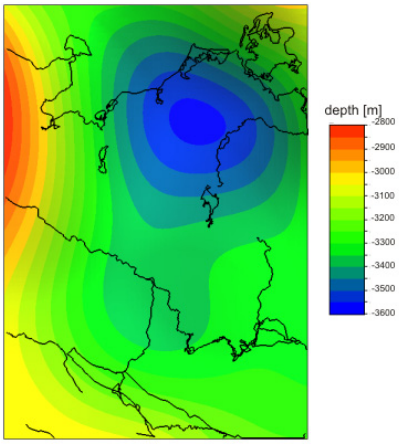

Figure 4: Depth to the Moho discontinuity used in the thermal simulation, after Tesauro et al. (2008)

Constraining the bottom boundary condition is more complex since very little information is available about its structure, composition and geometry. Results from previous lithospheric-scale thermal models (Kukkonen et al., 1999) have suggested that using a free lower boundary condition yields considerable higher uncertainties (systematic errors) than using constant temperature respectively. Accordingly, in the present study the base of the thermal model is approximated by the 1300°C isotherm (e.g. Turcotte and Schubert, 2002). Different seismological models have been tested to constrain the depth and the geometry of the Lithosphere-Asthenosphere isothermal Boundary (LAB). The final LAB model adopted in the study is the one as published by Artemieva et al. (2006), see Figure 5. This model provides the best fit with the observed heat flow density distribution taking into account the plausible range of variability for rock properties.

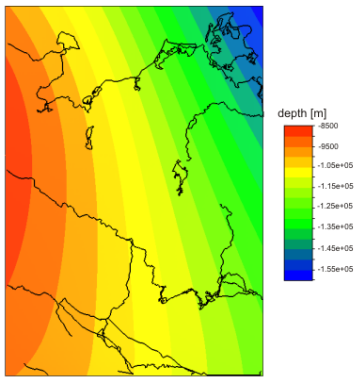

Figure 5: Depth to the LAB isothermal boundary as adopted in the numerical simulation, after Artemeieva et al. (2006)

In lithospheric forward thermal modeling, values of the different influencing thermal transport properties must be assigned to each layer and/or domain in the model. Due to the natural geological heterogeneity, there is a wide range of variation for rock properties, the degree of uncertainty increasing considering deeper crustal or mantle layers. As shown by previously random inverse (Monte Carlo) studies (e.g. Jokinen & Kukkonen, 1999), uncertainties of model parameters are directly transported to uncertainties of calculated temperature and heat flow density. In the present study, physical properties are considered constant within each specific layer as illustrated in Table 1. The resulting model is able to differentiate the main stratigraphic layers with depth while it does not fully quantify the effects related to the lithological stratification within each geologic unit.

Table 1: Thermal properties of rocks used for the numerical siulation of the regional thermal field in the NEGB, after Norden and Förster (2006) and Norden et al. (2008).

Stratigraphic unit		Thermal conductivity [$Wm^{-1}K^{-1}$]	Radiogenic heat production [$10^{-7}Wm^{3}$]
Cenozoic		1.5	9
Upper Cretaceous		1.9	6
Lower Cretaceous		2.0	15
Jurassic		2.0	15.5
Triassic (Keuper)		2.3	16
Triassic (Muschelkalk)		1.85	10
Triassic (Buntsandstein)		2.0	18
Upper Permian (Zechstein)		4.5	4
Lower Permian, Rotliegend	Elbe Subgroup	3.2	14
	Mirow Formation	3.7	14
	Parchim Formation	3.3	14
Permo-Carboniferous volcanics		2.5	21
Upper crystalline crust		3.1	25
Lower crystalline crust		2.2	1
Upper Mantle		4.1	0.1

The modelled temperature distributions are then validated by direct comparison with published temperature-vs-depth maps (e.g. Hurtig et al., 1992, Norden et al., 2008; Norden & Förster, 2006). Although geotherm calculations are very sensitive to variations in surface heat flow density values, to the authors' knowledge no efforts were made in the past to model the heat flow distribution in the NEGB. To overcome this problematic situation, additional numerical simulations of the surface heat flow distribution are carried out. Here and in the remain of the paper, surface heat flow refers to the vertical component of the heat flux vector calculated at each nodal point of the finite element grid using nodes at and immediately below the top slice of the model plus the heat budget contribution from the underlying strata taking into account radiogenic heat contribution as well. The modeled surface heat flux is compared to observed surface heat flow values (e.g. Hurtig et al., 1992; Norden et al., 2008). To estimate the influence of possible variations of the main physical parameters on the temperature and heat flow distribution, relative simple sensitive analyses with regard to the chosen physical properties are carried out. Thermal conductivities and heat production rates are varied following a trial-and-error approach, the calibration criterion given by the correspondence between computed and observed surface heat flow values. More detailed models, with spatial variations of thermal conductivities as a function of both temperature (including both phonon conduction and radiative contribution) and pressure corresponding to the available petrophysical database are under consideration. As a working example, Figure 6 and Figure 7 show calculated temperature distributions at selected constant depth levels. The computed geothermal field is characterized by both large-scale and small-scale anomalies. As clear by inspecting Figures 6a and Figure 6b, the shallower thermal field (down to about 5 km depth) is strongly influenced by (a) the geometry of the salt layer, (b) the burial depth of the top of the salt, and (c) the related heat budget contributions of the overburden. At 3 km depth (Figure 6a), the lowest temperatures are found all along the basin margins while relative high temperatures characterize the basin depocentre. Given the purely conductive nature of

the system, this asymmetrical thermal pattern reflects the spatial variations in the thickness of the structural layers and the related variations of the thermal conductivity field. Low temperatures are found in areas where sediment thickness decreases and where the thickness of the crust increases. This is due to the contrasts between the relative high thermal conductivity of the crystalline crust with respect to the lower conductivity values of sedimentary rocks.

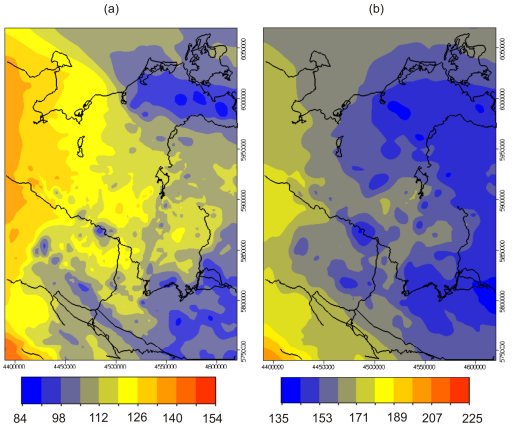

Figure 6: Shallow temperature distribution [°C] at constant depths. (a) Depth = – 3 km (above the salt); (b) Depth = -5 km (just below the salt)

In contrast, higher temperatures (up to 140 °C) are found in spatial correlation with salt margins or with regions where the supra-salt succession is relatively thick (about 4 km thick). In the latter case, conduction of heat into areas where the thickness of the sediments is relatively high raises the temperature at the base of the sedimentary succession, thermal blanketing. The temperature distribution at 5 km of depth (Figure 6b) is the result of two concurrent processes: increased heat transfer due to the high thermal conductivity of salt and the warming effect of the overburden. This interaction results in a broader area of low temperature with respect to Figure 6a correlating with areas of maximum salt thickness and only minor halokinesis. On the other hand, under regions of thick Zechstein overburden this cooling effect is strongly reduced. At greater depths, starting from about -10 km depth, the thermal field shows almost no memory of the shallow structures (Figure 7a, and Figure 7b). Lateral variation in the geothermal field parallel the integrated variations of the crust-to-mantle as well as of the isothermal LAB boundary.

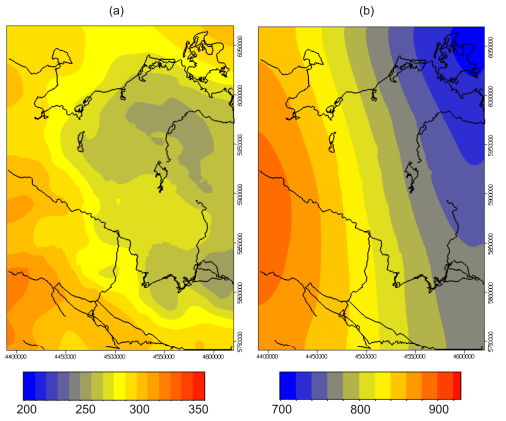

Figure 7: Temperature distributions [°C] at constant depths. (a) Depth = -10 km; (b) Depth = -50 km

The observed surface heat flow in the basin is highly heterogeneous, with areas of increased heat flow adjacent to areas of lower heat flow, e.g. Hurtig et al. (1992). Figure 8 illustrates the computed heat flow at the near-surface. A relative good agreement in regional trends and overall magnitudes of heat flow density is found. Surface heat flow values vary in a range from minima of about 40 to 60 mWm^{-2} to average maxima of 80 to 90 mWm^{-2} reaching locally 100 mWm^{-2}. The complex distribution of surficial heat flow reflects the near-surface temperature pattern as shown in Figure 6a, and Figure 6b. An increase in heat flow values is found toward the southern and western margins of the basin. Locally, the modelled heat flow anomalies can be attributed to salt diapirism and thermal refraction effects. Local increase in heat flow under areas of relative thick salt thickness is related to the salt-induced chimney effect. According to the high thermal conductivity of the salt, heat flow tends to be focused within the salt dome leading to an increase in heat flow density and temperature values above it. Recently, Norden et al. (2008) constrained heat flow to range from 60 to 91 mWm^{-2} with a mean of 77 ± 3 mWm^{-2}. Though too sparse for mapping purposes, the database from the study of Norden et al. (2008) can be used to constrain regional features and the range in variability of the surface heat flow. From the modelling results, an average heat flow value of 70 mWm^{-2} is derived. The calculated surface heat flow underestimates the values from the study of Norden et al (2008). The discrepancy can be attributed to local changes in the crustal composition and effects related to structural anisotropy that are not completely resolved by the present formulation. At the same time geometry and magnitudes of some of the positive heat flow anomalies from the study by Norden et al. (2008) (see their Figure 3) are not resolved by the modelling results. These local small-scale positive anomalies in the heat flow distribution could result from a combination of conduction and advective heat transport due to deep circulating fluid flow moving basement heat flow to the surface.

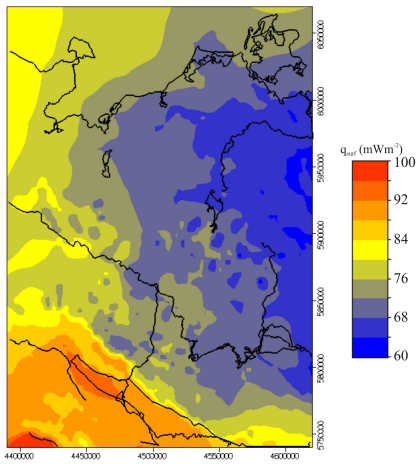

Figure 8: Calculated surface heat flux

3. COUPLED FLUID AND HEAT FLOW

The results from the modelling study presented in the previous section show a relative good agreement with regard to the general trends in the surface heat flow density and thermal structure. However, the role of convective heat transport as additional source of the heat flow distribution was not accounted for. On one hand, basin thermal budgets are dominated by heat conduction into the sedimentary pile from the underlying crystalline crust. On the other hand, heat flow across the base of the sedimentary sections may be strongly affected by an advective transport component

due to groundwater circulation. To correctly investigate convection and conduction contributions on the thermal and heat flow structure, three dimensional FE modeling of the fully coupled fluid flow and heat transport equations are carried out. To attempt a detailed hydrothermal interpretation of the convective system in the NEGB the convective flow beneath the Zechstein salt layer is not addressed in this part of the study. Consequently, the structural model integrates the top pre Zechstein layers as derived form the work by Scheck (1997). Table 2 (at the end of the manuscript) provides the physical parameters assigned to the respective layers. The coupled system of equations is numerically solved by the use of the commercial software package FEFLOW®. The equations describing thermal convection in a saturated porous media are governed by three partial differential equations based on the Darcy's law and mass and energy conservation laws, e.g. Nield and Bejan (2006). The system of flow equation with variable fluid density (ρ^f) and viscosity (μ^f) is given by (a) the mass conservation of the fluid:

$$\frac{\partial\left(\varepsilon\rho^f\right)}{\partial t}+\nabla\cdot\left(\rho^f\mathbf{q}^f\right)=\rho^f Q_\rho \qquad (2)$$

(with ε being the porosity, ρ^f the mass density of the fluid, $\mathbf{q}^f$ the specific discharge (Darcy's velocity) and Q_ρ the sink/source mass term) and by (b) the generalized Darcy's law:

$$\mathbf{q}^f=-\mathbf{K}\left(\nabla h+\frac{\rho^f-\rho_0^f}{\rho_0^f}\frac{\mathbf{g}}{g}\right) \qquad (3)$$

(where $\mathbf{K}$ is the hydraulic conductivity tensor of the porous media given by $\mathbf{K}=\frac{\rho_0^f g}{\mu^f}\mathbf{k}$, with $\mathbf{k}$ permeability tensor, and $\mathbf{g}$ is the gravity acceleration). Eq. 3 is written in terms of hydraulic head rather than pressure as primary variable. Under the assumption of thermal equilibrium between the medium and the fluid and if density and porosity gradients are neglected, applying the law of energy conservation yields to the following heat transfer equation:

$$(\rho c)_{fs}\frac{\partial T}{\partial t}+\rho^f c^f\nabla\cdot\left(\mathbf{q}^f T\right)-\nabla\cdot(\boldsymbol{\lambda}\nabla)=Q_T \qquad (4)$$

(with $(\rho c)_{fs}$ being the specific heat capacity of the fluid (f) plus solid (s) phase system as

$$(\rho c)_{fs}=\left[\varepsilon\rho^f c^f+(1-\varepsilon)\rho^s c^s\right] \qquad (5)$$

Q_T the heat source function, and $\boldsymbol{\lambda}$ being the equivalent thermal conductivity tensor of the fluid and porous medium. It incorporates dispersion effects in the fluid and heat transport for both the solid and fluid phase as:

$$\boldsymbol{\lambda}=\rho^f c^f\left[\alpha_T\sqrt{\left(q_i^f q_i^f\right)}\mathbf{I}+(\alpha_L-\alpha_T)\frac{q_i^f q_i^f}{\sqrt{\left(q_i^f q_i^f\right)}}\right]+ \qquad (6)$$
$$+\left[\varepsilon\boldsymbol{\lambda}_{cond}^f+(1-\varepsilon)\boldsymbol{\lambda}_{cond}^s\right]\mathbf{I}$$

where α_L and α_T are respectively the longitudinal and transversal dispersion lengths, $\boldsymbol{\lambda}_{cond}^f$ and $\boldsymbol{\lambda}_{cond}^s$ the thermal conductivity of the fluid and solid phase, and $\mathbf{I}$ is the unit matrix). The set of these balance equations are coupled by proper equations of state establishing the dependence of the fluid density and viscosity on the primary variables. In FEFLOW® the fluid density is expressed as a linear polynomial function of temperature and pressure as:

$$\rho^f=\rho_0^f\left[1-\bar{\beta}(T-T_0)+\bar{\gamma}(h-h_0)\right] \qquad (7)$$

where $\bar{\beta}=\frac{1}{\rho^f}\frac{\partial\rho^f}{\partial T}\Big|_p$ is the thermal expansion coefficient at constant pressure condition, and $\bar{\gamma}=\frac{1}{\rho^f}\frac{\partial\rho^f}{\partial h}\Big|T$ is the coefficient of fluid compressibility at constant temperature condition. Both coefficients can be either considered constant or functions of pressure and temperature, see Magri (2004) for more details. The dependence of the fluid dynamic viscosity upon temperature as implemented in FEFLOW® follows an empirical polynomial expression after Mercer and Pinder (1974):

$$\mu^f=\frac{1+0.7063\varsigma-0.04832\varsigma^3}{\mu_0} \qquad (8)$$

with $\varsigma=\frac{(T-150)}{100}$, and μ_0 the reference viscosity obtained from Eq. 6 when $T=T_0=150°C$. The commonly adopted Oberbeck-Boussinesq approximation has been employed in all the simulation runs. Following this approximation, density variations within the mass balance equation of the fluid phase (Eq. 2) are neglected. It follows that the system of equations is still coupled by the buoyant term in the Darcy's law (Eq. 3). In order to avoid numerical artefacts related to the FE scheme adopted which can lead to unphysical results, a grid convergence study has been carried out. The geometrical model to grid convergence to be established consisted of approximately one and a half million of elements with a horizontal resolution of half a kilometer and a variable vertical resolution to maintain a proper element aspect ratio. In all models the boundary conditions for the temperature are those obtained from the regional thermal study as explained in the previous chapter adapted properly to the geometry of the new finite element grid. The top boundary consists either of a fixed constant temperature of 8 °C or of an open Cauchy-type condition to let heat flowing out of the model. For the base of the model two different sets of boundary constraints have been tested, a Dirichlet boundary condition or a free boundary condition. Basal temperatures as obtained from the previous modeling range from 146 °C to 158 °C with a median value of 152 °C, whereas the basal heat flow values are in a range of 54 to 62 mWm^{-2} with a median value of 60 mWm^{-2}. The results from the numerical simulations (not shown here) suggested a relative great influence of the nature of the boundary conditions on the temperature field adopted. The effects related to the top distinct types of top boundary conditions are self-explaining with a fixed temperature along the top of the model prevents possible local heating and outflow of warmer water. Additionally, with the presence of an isothermal boundary no net advective component of the energy transfer is taken into account. In contrast, the effects of the bottom boundary condition can

be less constrained a priori. To investigate these aspects, different numerical simulations have been carried out in terms of the basal temperature condition chosen. All the other parameters affecting the flow system were not varied. From these preliminary studies it was found that a specified basal heat flow is more sensitive to fluid flow effects than a fixed basal boundary. The surface expression of this feature is a distribution of surface heat flow that is spatially differentiated for the two scenarios considered. On the contrary, absolute magnitudes of surface heat flow are poorly affected by the choice of the bottom boundary condition. The pressure top boundary condition is set in order to either incorporate (mixed thermal convection) or neglect (free thermal convection) the topography in the study area. The basal boundary is impermeable to fluid flow. Lateral boundaries are set close to both fluid and heat flow. The degree of coupling between the governing partial differential equations has been progressively increased following a step-like approach. The reason to start with less coupled models is related to their intrinsic simplicity thus providing a gentle introduction to the problem. At the same time, stability of the numerical solution with respect to the geometry and the nature of the system can be established with a great reduction in the CPU costs. Not shown in Table 2 is neither the ratio between longitudinal and transverse dispersivities and the corresponding absolute magnitudes. This is the case since little information is available to constrain these parameters for a large-scale system as the NEGB. Different test case solutions have been carried out varying the longitudinal/trasverse dispersivity from a minimum of 5/0.5 m (default values in Feflow) to a maximum of 500/50 m. Varying dispersivity of two orders of magnitude with respect to the default values does not affect the system behaviour. Mechanical dispersion plays only a minor component in the conduction-dispersion contribution to the flow and the numerical results are not sensitive to the assumed absolute values. Greater absolute dispersivities have been proven to stabilize the solution leading to smoother variations in the density distribution. For the sake of clarity, in the following the results obtained from one of these runs are described in detailed. This simulation represents the most coupled situation with fluid density and fluid viscosity taken as function of temperature and pressure and temperature respectively. Variations in thermal expansion and fluid compressibility in accordance to the current pressure and temperature conditions at each time step in the simulation run are also considered.

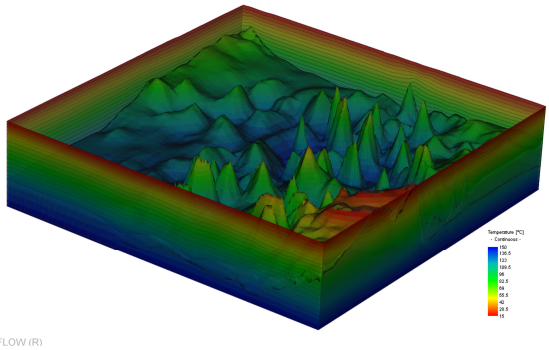

Figure 9: Temperature distribution on top of the salt layer and around the basin's boundary at the beginning of the simulation time, after 100 years

In Figure 9 the temperature distribution at the beginning of the simulation is plotted (after 100 years). Figure 9 provides an example of the first stages in the evolution through time of simulated temperatures above the Zechstein salt as well as isotherms all around the basin's boundaries. The thermal structure depicted in Figure 9 is typical of a conductive thermal regime with local thermal disturbances around the salt domes with isotherms bulging up/down at the top/bottom of the salt structures. After 50,000 years of simulation times, a change in the thermal distribution occurs, see Figure 10. A two-layered flow system develops with the quasi-impervious Muschelkalk unit providing the separation surface. Fluid convects only within the shallower (above the Muschelkalk) and more permeable strata creating relative small fluctuating convective cells. In contrast, heat conduction remains the dominant energy transport mechanism at deeper depths as indicated by the flat isotherms.

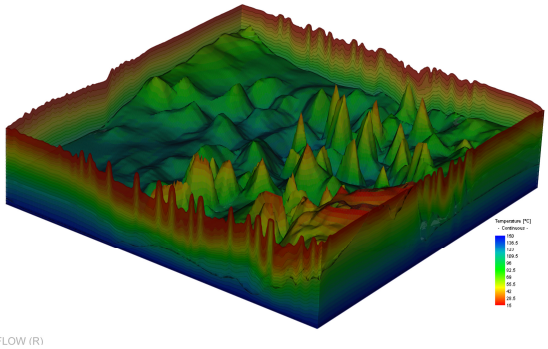

Figure 10: Temperature distribution above the Zechstein salt and isotherms along the boundaries of the study area after 50,000

The modeled convective system is not limited to restricted areas within the basin but it affects the entire basin as shown in Figure 11 where a cut out of the model area after 50,000 years is shown.

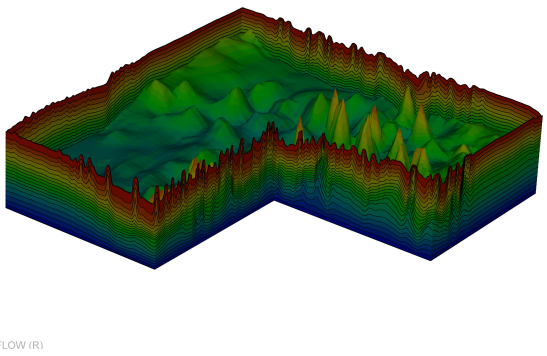

Figure 11: Cut out of the temperature evolution as shown in Figure 10 showing the basin-wide nature of the convective system affecting the area

Since no fault-related and/or high permeability preferential (vertical) conduits are considered, the simulated free convection pattern depends on the hydrogeologic conditions modelled. The main parameters affecting classical Rayleigh-type free convection in porous media are the aquifer thickness, basin geometry and permeability ratios between confining layers. Free thermal convection is favored by an increase in its thickness as well as vertical permeability. Under the hydrologic conditions considered the flow tends to be self-organized into different cells within the top layers where favorable thickness and

permeability conditions are met. Thermal disturbances are highly controlled by the geometry of the salt and tend to be preferentially localized above and around the salt domes. Due to the high thermal conductivity contrast between salt and the overlying sedimentary sections heat flow is focused along the salt structures (chimney effect) leading to higher temperatures near the edge of the salt structures. The unstable temperature distribution results in a thermally induced buoyant upward (downward) flow of hotter (colder) and less dense (denser) fluid on top of (at the edges of) the salt domes. According to the hydrologic conditions characterizing the salt overburden, this flow dynamics may favor the initiation of a (multi)cellular flow pattern.

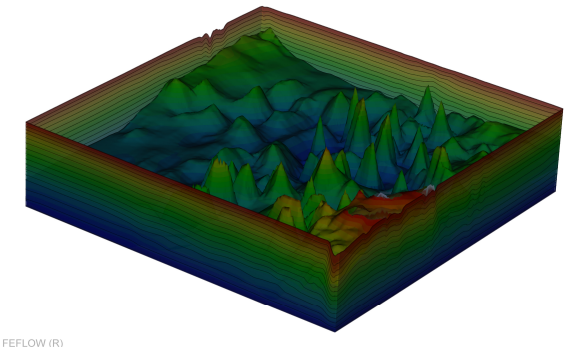

Figure 12: Temperature distribution after 50,000 years with an increase in permeability of three orders of magnitude of the shallower layers. Due to the new hydrogeologic setting, no convection occurs

To investigate the controlling effect of permeability ratios between confining layers with respect to the dominant flow mode, sensitivity analysis are carried out by changing the permeability values of the top layers. Though relative simple, it does not take into account anisotropy effects on the permeability field within a single layer, this study may provide an upper boundary for threshold permeability conditions for free convection to occur in the basin. Figure 12 illustrates the modeling results after 50,000 years of simulation. From this study a permeability value of $10^{-15/16}$ m^2 (=1/0.1 md) can be considered as a (upper) boundary between dominantly conductive (lower permeability values) or advective/convective (higher permeability) flow regime. Geologic media may exhibit total permeability ranges of more than 10 orders of magnitude. Given the reference permeabilities as shown in Table 2, the results show that a change of three orders of magnitude in the permeability range are enough to change the effective nature of the flow system.

CONCLUSION

A number of numerical simulations have been carried out in order to constrain the regional thermal structure and the basin-scale fluid dynamics for the area of the North East German Basin. The first part of the study deals with three dimensional modeling to investigate and characterize the recent regional conductive geothermal field. The aims of this preliminary study have been to investigate the interactions of the different rock properties and the variable thickness of the main geologic units with regard to the present thermal conductive structure. A good agreement between model results and observations has been found regarding regional trends. From the model results is clear that the rather complex pattern characterizing the modeled geothermal field and heat flow distribution mirrors the complex interaction of spatial distribution of thermal properties and layers' thickness. The shallow thermal field (up to a constant depth of approximately 5 km) is strongly influenced by the thickness and geometry of the salt layer, the burial depth of the top of the salt and the heat budget of the salt overburden. Surface heat flow may be regarded as the result of different processes acting at variable spatial and temporal scales. On the one hand the long wavelength character of the near surface heat flow distribution is strongly controlled by the deeper crustal structures. Local heterogeneities in the crustal structure and composition may be regarded as first-order controlling factors in explaining the observed positive anomalies in the distribution of heat flow. On the other hand, increased heat transfer in proximity of salt domes (chimney effect), thermal refraction due to conductivity contrasts as well as advective heat transfer processes due to deep circulating fluid flow may have a major impact at smaller spatial scales. To better investigate the role of convective heat transport, in the second part of the paper some results from fully coupled heat and fluid flow simulations have been discussed. The results on the long term behaviour of the system have given more than indications for the presence of a subsurface convective-dominated fluid system. Where favorable hydrogeologic conditions are encountered, stable convective multicellular convection may be sufficient to affect the regional density stratification and the thermal structure of the system. However, it is still to quantify whether and how the key characteristics of this convective system will be affected by taking into account solute effects on both the fluid density and viscosity. Simulations of fully coupled thermohaline flow regimes are currently under progress. Additionally, to study the role of structural and mechanical heterogeneities (e.g. faults) as well as to investigate the effects of the active stress regime and deformation mechanisms on the regional flow dynamics remain tasks for future researches. Nevertheless from the results obtain so far, it is clear that the spatial (basin-wide) and temporal scales of the convective fluid system make free thermal convection a major candidate among the processes affecting the NEGB.

REFERENCES

Artemieva, I.M., Thybo, H., and Kaban, M.K.: Deep Europe today: geophysical synthesis of the upper mantle structure and lithospheric processes over 3.5 Ga, In: Gee, D.G. and Stephenson, R.A. (eds.) 2006. European Lithosphere Dynamics, *Geological Society, London, Memoirs*, **32**, 11-41.

Bayer, U., Scheck, M., and Koehler, M.: Modeling of the 3D thermal field in the northeast German basin, *Geol Rundsch*, **86**, (1997), 241-251.

Bayer, U., Scheck, M., Rabbel, W:, Krawczyk, C.M:, Götze, H.-J., Stiller, M., Beilecke, Th., Marotta, A.-M., Barrio-Alvers, L:, and Kuder, J.: An integrated study of the NE German Basin, *Tectonophysics*, **314**, (1999), 285-307.

Hurtig, E., Cermàk, V., Haenel, R., and Zui V.: Geothermal Atlas of Europe, *Hermann Haack Verlagsgesellschaft mbH, Geographisch-Kartographische Anstalt Gotha*, (1992).

Jokinen, J., and Kukkonen I.T.: Inverse simulation of the lithospheric thermal regime using the Monte Carlo method, *Tectonophysics*, **306**, (1999), 293-310.

Kukkonen, I.T., Jokinen, J., and Seipold, U.: Temperature and pressure dependencies of thermal transport properties of rocks: implications for uncertainties in

thermal lithosphere models and new laboratory measurements of high-grade rocks in the central Fennoscandian Shield, *Surveys in Geophysics*, **20**, (1999): 33-59.

Magri, F.: Derivation of coefficients of thermal expansion and compressibility for use in FEFLOW, *WASY White papers*, **III**, (2004), 13-23.

Magri, F., Bayer, U., Clausnitzer, V., Jahnke, C:, Diersch, H.-J., Fuhrmann, J., Möller, P., Pekdeger, A., Tesmer, M., and Voigt, H.: Deep reaching fluid flow close to convective instability in the NE German basin – results from water chemistry and numerical modelling, *Tectonophysics*, **397**, (2005), 5-20.

Mercer, J.W., and Pinder, G.F:: Finite element analysis of hydrothermal systems. Finite element methods in flow problems, Proceedings 1st Symposium, Swanseea, ed. Oden, J.T. et al., *University of Alabama Press*, (1974), 401-414.

Nield D.A., Bejan, A.: Convection in porous media, 3rd edition, *Springer*, (2006).

Norden, B., and Förster, A.: Thermal conductivity and radiogenic heat production of sedimentary and magmatic rocks in the Northeast German Basin, *AAPG Bulletin*, **90(6)**,(2008), 939-962.

Norden, B., Förster, A., and Balling, N.: Heat flow and lithospheric thermal regime in the Northeast German Basin, *Tectonophysics*, **460**, (2008), 215-229.

Scheck, M.: Dreidimensionale Strukturmodellierung des Nordostdeutschen Beckens unter Einbeziehung von Krustenmodellen, *Scientific Technical Report STR97/10*, GeoForschungsZentrum Potsdam (1997).

Simmons, C.T., Fenstemaker, T.R., and Sharp Jr., J.M.: Variable-density groundwater flow and solute transport in heterogeneous porous media: approaches, resolutions and future challenges, *Journal of Contaminant Hydrology*, **52**, (2001), 245-275.

Tesauro, M., Kaban, M.K., and Cloetingh, S.A.P.L.: EuCRUST-07: A new reference model for the European crust, *Geophysical Research Letters*, **35**, (2008), L05313, doi:10.1029/2007GL032244. Available from open sources at: ftp://ftp.agu.org/apend/gl/2007gl032244.

Turcotte, D., Schubert G.: Geodynamics, 2nd edition. *Cambridge University Press.*

Zhao, C., Hobbs B.E:, Ord, O., Peng, S., Mühlhaus, H.B., and Liu, L.: Theoretical investigation of convective instability in inclined and fluid-saturated three-dimensional fault zones, *Tectonophysics*, **387**, (2004), 47-64.

Table 2: Physical parameters adopted for the coupled fluid and heat simulations, after Magri et al. (2005), Scheck (1997). Fluid thermal conductivity and heat production rates are the same as in Table 1. Due to the poor constraints on other fluid thermal properties constant values as default in the FEFLOW simulator has been adopted for heat capacity and thermal conductivity.

Geologic layer	Flow transport properties		Heat transport properties	
	Permeability $\boldsymbol{\kappa}$ [10^{-12}m^2]	Porosity ε [%]	Rock density ρ^s [kgm^{-3}]	Rock heat capacity c^s [kJ(kgK)$^{-1}$]
Cenozoic	1	23	2670	1.18
Upper Cretaceous	0.1	10	2400	1
Lower Cretaceous	0.1	13	2700	1.18
Jurassic	0.1	13	2700	1.18
Upper Triassic (Keuper)	0.01	6	2700	1.18
Middle Triassic (Muschelkalk)	1e^{-6}	~0	2400	1
Lower Triassic (Buntsandstein)	0.01	4	2670	1.18
Zechstein salt	Impervious ~ 0	~0	2160	0.84
Basement	Impervious ~ 0	~0	2670	1.18